# Acoustic beam splitting in a sonic crystal around a directional band gap*

Ahmet Cicek[a)†], Olgun Adem Kaya[b)], and Bulent Ulug[c)]

[a)] Department of Physics, Faculty of Arts and Sciences, Mehmet Akif Ersoy University, Campus 15100, Burdur/Turkey
[b)] Department of Computer Education and Educational Technology, Faculty of Education, Inonu University 44280, Malatya/Turkey
[c)] Department of Physics, Faculty of Science, Akdeniz University, Campus 07058, Antalya/Turkey

(Received 12 March 2013; revised manuscript received 1 April 2013)

Beam splitting upon refraction in a triangular sonic crystal composed of aluminum cylinders in air is experimentally and numerically demonstrated to occur due to finite source size, which facilitates circumvention of a directional band gap. Experiments reveal that two distinct beams emerge at crystal output, in agreement with the numerical results obtained through the finite-element method. Beam splitting occurs at sufficiently-small source sizes comparable to lattice periodicity determined by the spatial gap width in reciprocal space. Split beams propagate in equal amplitude, whereas beam splitting is destructed for oblique incidence above a critical incidence angle.

**Keywords:** sonic crystal, directional band gap, source size, beam splitting

**PACS:** 43.20.El, 43.40.Fz, 43.58.Fm **DOI:** 10.1088/1674-1056/22/11/114301

## 1. Introduction

Sonic crystals (SCs) have many applications, such as interferometry[1] and (de)multiplexing[2–4] in which splitting acoustic waves in an equal amplitude with controllable phase difference may be required. An impinging wave can be split either by deliberately disturbing crystal periodicity[5–8] or making use of band structure concepts, so that the crystal is kept intact.[9–15]

Y- and T-shaped branches of linear defect waveguides in two-dimensional (2D) SCs[5] fall in the first category. Highly-directional emission from a point-like source through a defect state is another means of splitting over pre-defined paths.[6,7] Furthermore, self-collimated waves[16–18] can be split at the input of a SC composed of rotated elliptical scatterers so that mirror symmetry about the acoustic axis exists.[8]

In the context of the second category, SCs are utilized as a whole. For instance, directional acoustic radiation from a point source embedded in a square SC can be split over four orthogonal self-collimation paths, provided that flat square-like equi-frequency contours (EFCs) exist.[9] Appearance of different EFCs for different mode types in a 2D SC can be utilized for separating shear wave modes on a slab.[10] Other approaches facilitate coupling into more than one spatial mode of a SC, through either overlapping bands, leading to negative birefraction,[11] or translational symmetry in the reciprocal space.[12–15] In the former, waves are split at the input interface, while the latter involves excitation of multiple modes equivalent by reciprocal lattice vector ($\boldsymbol{G}$) translations, which develop different phases and couple back into distinct modes of the host. In both schemes, propagation directions of the split waves can be deduced from the inspection of EFCs. However, splitting capability depends on the angle of incidence ($\theta_{\rm in}$). Moreover, equal distribution of acoustic intensity over the branches is not guaranteed.

Excited states in a SC are generally determined through the use of construction lines, ruled by the requirement that parallel component of the wave vector across an interface is conserved. This is validated as long as the transverse extent of the incident wave is sufficiently large compared to crystal period, so that the waveform can approximately be represented by a Dirac delta function in the Fourier space. However, limited source size may be crucial in achieving specific applications, such as non-diffractive propagation.[17] For instance, shear waves incident in a direction on which sharp corners of EFCs reside can be split by a triangular SC if the source width is reduced.[19] Moreover, source width and its corresponding angular spread in the reciprocal space should be taken into account if the frequency and the propagation direction fall in an angular band gap,[20,21] which can be utilized for spatial filtering of sound beams[21] or tuning beam profile behind the crystal.[20] Furthermore, directional band gaps,[22] a range of wave vectors around a high-symmetry direction for which no spatial modes exists in the band structure of the SC, can be utilized in many applications, such as unidirectional sound transmission.[22,23] Incoming waves should either be tilted or have sufficiently small transverse sizes to circumvent directional band gaps.

In this work, acoustic beams with transverse size comparable to lattice periodicity are split at the input interface of

*Project supported by Akdeniz University Scientific Research Projects Coordination Unit.
†Corresponding author. E-mail: ahmetcicek@mehmetakif.edu.tr
© 2013 Chinese Physical Society and IOP Publishing Ltd 

a 2D SC by means of a directional band gap. Beam splitting without disturbing the lattice periodicity is demonstrated both numerically and experimentally. Splitting properties are examined with respect to the source width and the angle of incidence.

## 2. Experimental setup and computational methods

A triangular SC with a rigid isotropic basis in the air whose Wigner–Seitz cell, geometrical parameters, and unit vectors are depicted on the top left of Fig. 1(a), is considered. The scatterers are aluminum cylinders with 2700-kg/m$^3$ mass density, while the air density is 1.21 kg/m$^3$. Cylinders are mounted between two Delrin plates, (Fig. 1(b)), drilled with less than 1% standard deviation in lattice constant and radii, which are $a = 25$ mm and $r = 10$ mm, respectively. The longitudinal speeds of sound in the two media are taken as $c_{\rm Al} = 6420$ m/s and $c_{\rm air} = 343$ m/s. An $20\times10$ arrangement of the SC, depicted in Fig. 1(a), with the long side being normal to the [11] direction is considered.

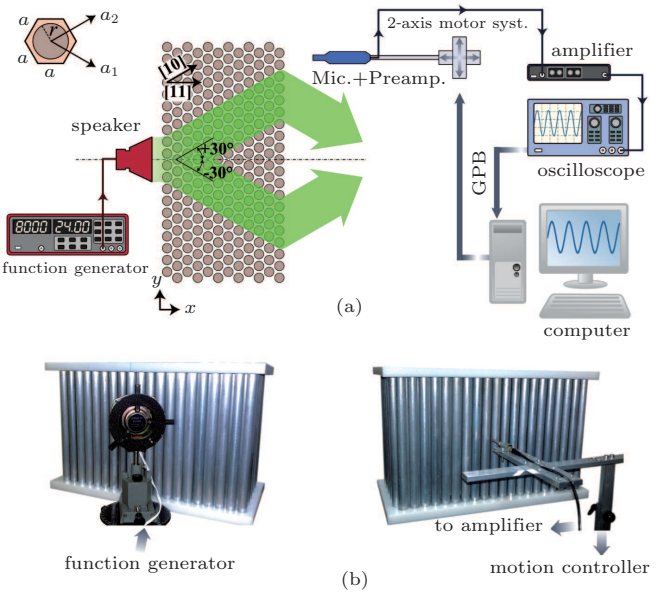



**Fig. 1.** (color online) Sketch of the experimental setup along with the Wigner–Seitz unit cell of the triangular SC (top left) (a) and photographs of the SC with speaker (left) and microphone (right) on opposite faces. (b) The transparent arrows on the SC in (a) represent the paths of the split beams.

Experiments are carried out by exciting the SC through loudspeakers of different diameters and recording pressure field distribution on the opposite side of the SC by a microphone. The experimental setup is sketched in Fig. 1(a), whereas figure 1(b) provides photographs of the SC. The setup is similar to the one utilized by Feng *et al.*[24,25] in the demonstration of negative refraction by a 2D SC. Speakers are driven by a sine wave at 8.00 kHz using a Uni-T UTG 9005C function generator, whose frequency stabilization is better than 0.1%. Pressure distribution is recorded with a minimal distortion on the opposite SC face by using a GRAS 40BF 1/4″ pre-polarized free-field microphone connected to a short 1/4″ GRAS 26AB pre-amplifier powered by a GRAS 12AK power module, which provides further amplification in 4-Hz-100-kHz frequency range. The amplified signals are then fed into a Tektronix TDS3052B 500-MHz digital oscilloscope, whose output is averaged over 32 consecutive root-mean square (RMS) voltage readings. The microphone-amplifier-oscilloscope system is synchronized with a computer-driven two-axis stepper-motor system, where the microphone position is scanned on the $xy$ plane over a 415 mm×95 mm ($16.6a\times3.8a$) area by 1.75 mm and 1.0 mm steps in $x$ and $y$ directions, respectively. Environmental noise and reflection interference from laboratory walls, etc, are minimized by acoustic absorbers not shown in Fig. 1(b) for clarity.

The acoustic response of the SC is investigated through the inspection of the EFCs on the second acoustic band calculated by means of the plane-wave expansion (PWE) method[8] with 961 ($31\times31$) plane waves. A sample frequency of 8.00 kHz which falls in the second band is chosen in experiments and 2D steady-state finite-element method (FEM) simulations implemented in COMSOL MultiPhysics package. The computational domain in FEM simulations, discretized in an adaptive-meshing scheme with a maximum mesh size of 1.0-mm ($a/25$), is surrounded by a perfectly-matched layer absorbing boundary.[26]

Simulations are carried out by considering a monochromatic quasi-plane wave traveling along the $+x$ direction with a wave vector (angular frequency) $k_0$ ($\omega_0$). Beam splitting capability of the SC at 8.00 kHz is examined after exciting the SC by sources with different sizes, whose transverse profiles (in the $y$ direction) are products of rectangular and Gaussian envelopes, which can be written as

$$p(x,y,t) = p_0\Pi(y;h)\mathrm{e}^{-y^2/\sigma^2}\mathrm{e}^{\mathrm{i}(\omega_0 t - k_0 x)}, \tag{1a}$$

where $p_0$ is a constant and $\sigma$ is the $1/e$ half width of Gaussian. $\Pi(y;h)$ is Heaviside $\Pi$ function defined as

$$\Pi(y;h) = \begin{cases} 0, & |y| > h; \\ \dfrac{1}{2}, & |y| = h; \\ 1, & |y| < h, \end{cases} \tag{1b}$$

where $h$ is the half width of the source. The choice of Eq. (1a) to represent incident waves rests in the requirement to numerically reproduce experimental beam profiles in Fig. 5(b) of the speakers. The source spans a range of roughly $2\pi/h$ along the $k_y$ direction in reciprocal space and its span determines whether spatial modes around a directional band gap could be excited.

## 3. Band structure of the sonic crystal

The first three acoustic bands of the SC are presented in Fig. 2(a). The first and second bands approach at the $K$ point at 6.65 kHz, whereas there is a full band gap between the second and third bands between 12.40 kHz and 14.20 kHz, see Fig. 2. Thus, the possibility of birefraction due to the band overlap[11] is eliminated and the observed beam splitting behavior is due solely to circumventing a directional band gap, as will be discussed below. Transmittance along the [11] direction calculated through FEM simulations is below $-20$ dB within the band gap, where it becomes as low as $-48$ dB in the middle of the gap, see Fig. 2(b). Our attention is confined to the second band which lies between 6.65 kHz and 12.40 kHz. The frequency, 8.00 kHz, at which the experiments are carried out is marked by the horizontal dashed lines in Fig. 2. The calculated total transmittance at this frequency is $-4.6$ dB, a relatively high value.

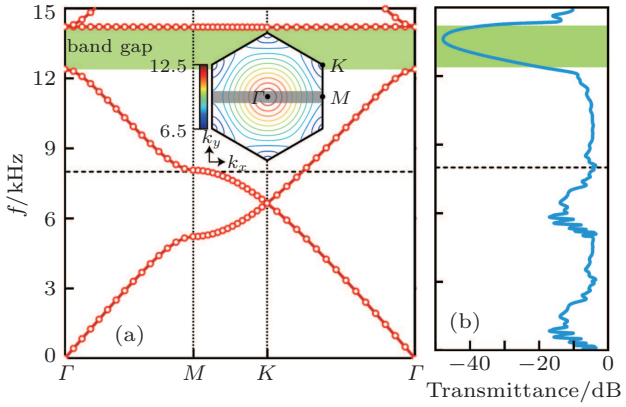



**Fig. 2.** (color online) Band structure of the SC computed by using the PWE method (a) and calculated transmittance spectrum along the [11] direction (b). The inset in (a) presents the first Brillouin zone and the high-symmetry points, as well as the equi-frequency contours within the second band. The dashed lines and the rectangular areas in (a) and (b) represent 8.00 kHz and the band gap, respectively.

The EFCs within the second band, centered either on the $\Gamma$ or $K$ point, are presented in the inset of Fig. 2(a) in the reduced-zone scheme. The $K$-centered EFCs for $f \leq 8.07$ kHz lead to appearance of a directional band gap along the $\Gamma M$ direction, whose width varies with frequency. The rectangular patch in the inset of Fig. 2(a) depicts the directional band gap at 8.00 kHz, whose half width is $\Delta k_{ym} = 0.14\pi/a$. A quasi-plane incident wave along the $\Gamma M$ direction with the transverse extent ($d$) much larger than $a$ cannot find any spatial modes to couple to due to the directional band gap.

The above analysis fails if $d$ is small, especially if $d < \pi/\Delta k_{ym}$, which is $7.14a$ at 8.00 kHz. In this case, the source possesses a finite extent along the transverse ($k_y$) direction in the reciprocal space and coupling into the spatial modes around the directional band gap could be possible. This is the mechanism behind the beam splitting scheme in this work and is pictorially demonstrated in Fig. 3.

The plot on the left of Fig. 3 is the distribution of Fourier components of the source defined in Eq. (1a) when $h$ goes to infinity and $\sigma = 2a$, so that the transverse source profile is Gaussian. The wave is assumed to impinge on the (11) face of the SC normally. The full width at half maximum (FWHM) of the distribution is $2\pi\sqrt{\ln 2}/\sigma = 0.83\pi/a$, so that it is greater than the directional band gap width, $0.28\pi/a$. This source can find spatial modes of the SC at 8.00 kHz to couple to and, thus, the directional band gap can be circumvented. This is demonstrated by drawing the construction lines at the FWHM limits denoted in Fig. 3. The construction lines intersect the EFCs at four points, each. The hollow arrows, which make $\pm 30^\circ$ with the $\Gamma M$ direction, on the EFCs in Fig. 3 indicate that two independent modes are excited in the SC and follow distinct self-collimated paths due to flatness of the EFCs around the construction lines, Fig. 3. The excited modes on the contours on the right in Fig. 3 are not demonstrated since they are equivalent to the indicated modes by symmetry. Considered all possible construction line pairs, it can be deduced that all excited modes for this particular source are self-collimated and are parallel for each split branch, leading to appearance of only two distinct branches suggested in Fig. 1(a). Thus, beam splitting by circumventing the directional band gap with a sufficiently-small source is established.

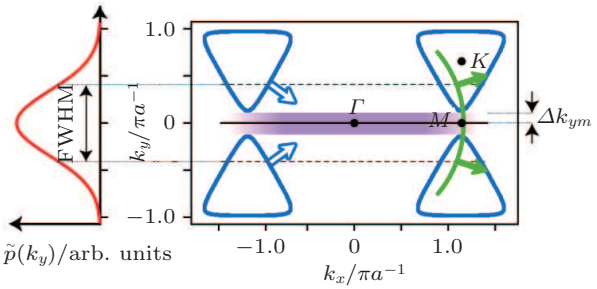



**Fig. 3.** (color online) Demonstration of beam splitting around the directional band gap along the $\Gamma M$ direction through the EFCs at 8.00 kHz. The circular arc on the right represents the EFC of air at the same frequency. The hollow and solid arrows on the dashed horizontal construction lines represent the propagation directions of the spatial modes in the SC and air, respectively. The horizontal patch denotes the limits of the directional band gap.

The split branches in Fig. 3 are negatively refracted at the input interface of the SC in Fig. 1. They are negatively refracted once more at the output interface when they couple back into air. The propagation directions through air can be determined by investigating the intersections of the construction lines in Fig. 3 with the EFC in air, which is represented by the circular arc on the right of the figure. The outgoing branches depicted by the solid arrows make $\pm 18^\circ$ with the acoustical axis for the particular construction lines considered. However, since there are many excited modes in the SC on each contour, the branches going out into air are spread due to the curvature of the air EFC, although the spread is small as its curvature remains small between the construction lines.

The beam splitting ability is not limited to a single frequency of 8.00-kHz. From the EFCs in the inset of Fig. 2(a), $\Delta k_{ym}$ can be expected to increase as the frequency decreases since the corresponding contours become smaller around the $K$ point. Variation of $\Delta k_{ym}$ with frequency is presented in Fig. 4, where a smooth decrease with frequency is seen. The $\Delta k_{ym}$ value ($0.14\pi/a$) at 8.00 kHz is marked in Fig. 4 and it becomes $0.40\pi/a$ and $0.56\pi/a$ at 7.50 kHz and 7.00 kHz, respectively.

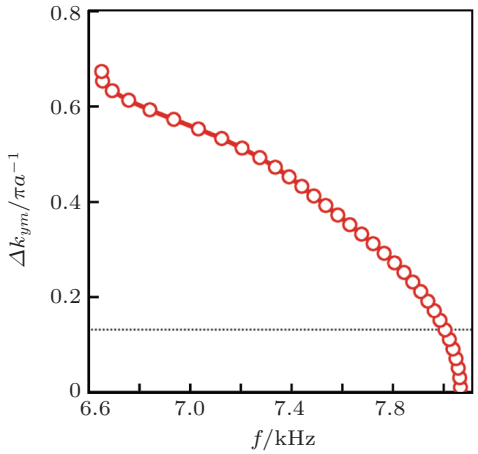



**Fig. 4.** (color online) Variation of the directional band gap half width in the second band of the SC with frequency. The horizontal dotted line indicates the value at 8.00 kHz.

The critical transverse source size for achieving beam splitting can be estimated as $d^{(\max)} = \pi/\Delta k_{ym}$. For a monochromatic normally-incident incident wave, $d^{(\max)}$ is calculated as $7.14a$, $2.50a$, and $1.79a$ at 8.00 kHz, 7.50 kHz, and 7.00 kHz, respectively, for the $\Delta k_{ym}$ values in Fig. 4. The Gaussian source with $\sigma = 2a$ could easily excite spatial modes of the SC in Fig. 3 at 8.00 kHz, while it could hardly excite any modes at 7.50 kHz and 7.00 kHz. Thus, source size is critical in the beam splitting capability of the SC at a given frequency. Moreover, not only the directional band gap width but also the EFC curvature increases as frequency decreases, see the inset of Fig. 2(a). Thus, the self-collimated character of the split branches in the SC is disrupted at smaller frequencies, even if sufficiently-small sources are employed.

## 4. Demonstration of beam splitting

Two electromagnetically-driven speakers with active diameters of 35 mm and 100 mm are employed in experiments. Free-field profiles of the speakers at 8.00 kHz are depicted in Fig. 5. The plots in Fig. 5(a) represent the distribution of acoustic intensity represented by the sound intensity level (SIL) calculated as SIL=$10\log_{10}(I/I_0)$ where $I_0$ is the maximum intensity in each case. The 35-mm-speaker field exhibits no side lobes, while they are visible for the one of 100 mm. Both speaker fields exhibit periodic maxima on their acoustic axes and distributions on vertical cuts coinciding with the maxima closest to the speakers are presented in Fig. 5(b).

The source-SC distances, indicated by the vertical lines in Fig. 5(a) fall in the near fields of both speakers whose Rayleigh distances are calculated as 22.60 mm and 184.80 mm, respectively. The choice is based on the fact that the acoustic source profile does not broaden significantly, so that the source size can be assumed constant. Under these conditions, equation (1a) is fitted to each profile in Fig. 5(b) with coefficient of determination ($R^2$) greater than 0.9. Calculated $d$ values for small and large speakers are $d_S = 48.0$ mm ($1.9a$) and $d_L = 72.5$ mm ($2.9a$), respectively, as depicted in Fig. 5(b). The corresponding $\sigma$ values are 32.7 mm ($1.3a$) and 40.0 mm ($1.6a$), respectively.

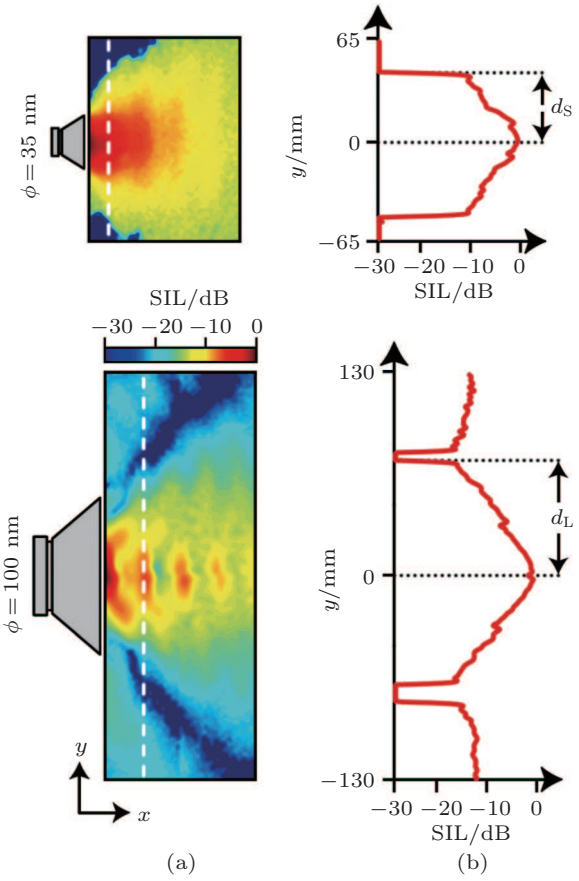



**Fig. 5.** (color online) Free-field acoustic intensity distributions of small (top) and large (bottom) speakers (a) and corresponding variations on the dashed vertical slices (b).

Propagation of waves at 8.00 kHz emanating from the above-mentioned speakers inside and outside the SC is presented in Fig. 6. Experimental and numerical source-SC distances are taken as 14.0 mm and 28.0 mm for the small and large speakers, respectively. Sources in simulations are defined by Eq. (1a), where $d$ and $\sigma$ values determined by curve fitting are stated above, to match experimental conditions.

Beam splitting immediately at the input interface of the SC is evident in Fig. 6(a), where numerically-obtained pressure field distribution inside the SC is presented. The two split branches possess equal intensity and make $\pm 30^\circ$ with the

acoustic ($x$) axis. The branches arriving at the output face suffer reflection losses, which can be reduced by cutting the output interface normal to the [10] direction to form an SC prism.

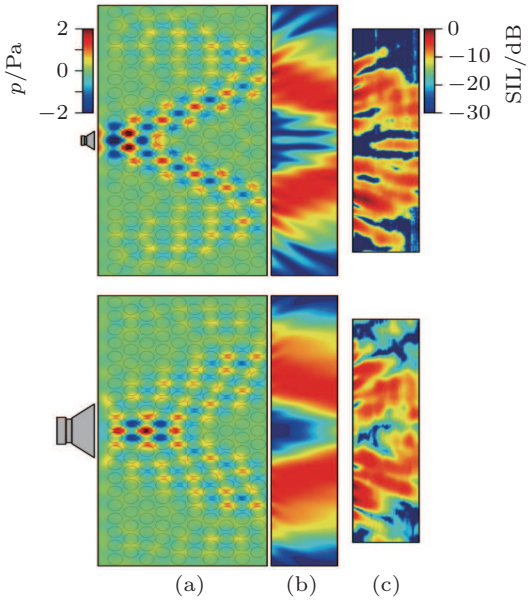



**Fig. 6.** (color online) FEM simulations of beam splitting in the SC (a), corresponding numerical acoustic intensity (SIL) distribution outside the SC (b), and the associated experimental data (c).

The split branches for the small source in Fig. 5(a) propagate in sharply-defined self-collimated paths. On the contrary, although being split on the expected paths, the branches for the large source do not propagate in a self-collimated manner. The discrepancy stems from the fact that the smaller source spans a larger extent along the $k_y$ direction in the reciprocal space and spatial modes on the flat portions of the EFC are overwhelmingly excited. As source size is increased, however, relative contribution of the modes on the rounded corners in Fig. 3 enhances. Beam splitting capability at 8.00 kHz diminishes in FEM simulations for the sources of $h > 5a$, and with decreasing frequency as $\Delta k_{ym}$ increases with decreasing frequency. Beam splitting occurs only for $h \leq 2a$ at 7.50 kHz, while it is not observed at 7.00 kHz even for a source with $h = 0.5a$.

Numerically-obtained field profiles outside the crystal depicted in Fig. 6(b) are presented as SIL for the ease of comparison with experimental data. Two outgoing waves negatively-refracted at the SC-air interface are visible, where the branches corresponding to small source are narrower. Moreover, corresponding branches for the two sources leave the SC at the same lateral positions. Experimental SIL data in Fig. 6(c) are consistent with the numerical data. The numerical and experimental outgoing branches into air leave the SC at approximately $\pm 4.5a$ and $\pm 4.0a$ for both sources with respect to the acoustical axis. Moreover, the corresponding spacings between the outgoing wave fronts are approximately 23 mm and 22 mm, respectively, which are close to half the wavelength in air, i.e., 42.88 mm. Although a single propagation direction cannot be assigned for the outgoing waves due to the spread discussed above, the numerical waveforms make approximately $\pm 17^\circ$ and $\pm 21^\circ$ for the small and large sources, respectively. The values are consistent with the propagation directions depicted by the solid arrows in Fig. 3. Propagation angles of the experimentally-obtained outgoing waves cannot be so easily evaluated. Nevertheless, the agreement between numerical and experimental data is satisfactory.

The beam splitting behavior of the SC should also be investigated for oblique incidence. Although the modes are excited symmetrically about the $\Gamma M$ direction for normal incidence as in Fig. 3, the symmetry is broken if $\theta_{\text{in}} \neq 0^\circ$. Considering an ideal plane incident wave with a very large transverse extent, the directional band gap in Fig. 3 can also be circumvented if $\theta_{\text{in}}$ is varied. In such case, a critical angle of incidence ($\theta_{\text{m}}$) beyond which couples into a SC mode in the vicinity of the directional band gap can be defined. To be specific, $\theta_{\text{m}}$ is calculated as $\pm 6.93^\circ$, $\pm 21.54^\circ$, and $\pm 33.57^\circ$ at 8.00 kHz, 7.50 kHz, and 7.00 kHz, respectively, for the investigated SC.

The splitting behavior in Fig. 6 should be destructed for oblique incidence for sufficiently large $\theta_{\text{in}}$, as only the modes below or above the $\Gamma M$ line would be excited. To demonstrate this, FEM simulation and experiment are carried out with the large (100 mm) speaker for $\theta_{\text{in}} = 30^\circ$. Figures 7(a) and 7(b) present the numerical results, while figure 7(c) depicts the experimental one.

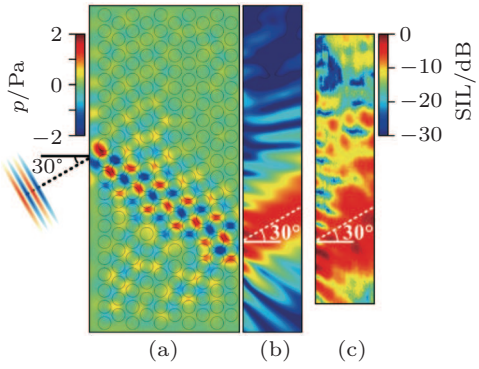



**Fig. 7.** (color online) Depiction of FEM simulation result for $\theta_{\text{in}} = 30^\circ$ at 8.00 kHz (a), with corresponding numerical (b) and experimental (c) acoustic intensity distribution data outside the crystal.

An obliquely-incident wave can couple into spatial modes on the EFC lobes above the acoustic axis in Fig. 3. Therefore, only downward-going wave components (making $-30^\circ$ with surface normal) are excited in the SC, (see Fig. 7(a)). Outgoing wave is negatively-refracted again at the SC-air interface and propagates in air parallel to the incoming one, (see Fig. 7(b)). The numerical and experimental data are again in good agreement with each other in terms of the emergence sites of the outgoing waves, $-5.5a$ and $5.0a$, respectively, below the acoustic axis, and the wavefront spacings (approximately half the wavelength). However, the wave spread

is more pronounced for the experimental outgoing wave in Fig. 7(c). Use of a vertically-longer speaker, whose acoustic field pattern is more uniform along $y$ direction, may be useful in improving the consistency between the numerical and experimental results in Figs. 7(b) and 7(c).

## 5. Conclusion

The splitting of acoustic waves in a triangular sonic crystal at specific frequencies for which a directional band gap appears along a principal direction, is experimentally and numerically demonstrated to take place if the source is sufficiently small. The split components propagate on paths making $\pm 30^\circ$ with the acoustic axis in equal amplitudes. The splitting behavior of the crystal is destructed for the oblique incidence above a critical angle.

## Acknowledgment

The authors are grateful to Prof. Dr. Battal CIPLAK for his kind permission to use the microphone system and Mr. Dincer TOSUN from Arma Industrial-Antalya/Turkey, for the construction of sonic crystal.

## References

[1] Sanchis L, Håkansson A, Cervera F and Sánchez-Dehesa J 2003 *Phys. Rev. B* **67** 035422
[2] Håkansson A, Sánchez-Dehesa J and Cervera F 2006 *Appl. Phys. Lett.* **88** 163506
[3] Pennec Y, Djafari-Rouhani B, Vasseur J O, Khelif A and Deymier P A 2004 *Phys. Rev. E* **69** 046608
[4] Vasseur J O, Bou M O, Robillard J F, Hladky-Hennion A C and Deymier P A 2011 *AIP Adv.* **1** 041904
[5] Li X and Liu Z 2005 *Phys. Lett. A* **338** 413
[6] Wu F G, Liu Z Y and Liu Y Y 2004 *Phys. Rev. E* **69** 066609
[7] Yao Z J, Yu G L, Wang Y S and Shi Z F 2009 *Int. J. Solids Struct.* **46** 2571
[8] Wu L Y and Chen L W 2007 *J. Phys. D: Appl. Phys.* **40** 7579
[9] Wen J, Yu D, Cai L and Wen X 2009 *J. Phys. D: Appl. Phys.* **42** 115417
[10] Ma P S, Kim H W, Oh J H and Kim Y Y 2011 *Appl. Phys. Lett.* **99** 201906
[11] Lu M H, Zhang C, Feng L, Zhao J, Chen Y F, Mao Y W, Zi J, Zhu Y Y, Zhu S N and Ming N B 2007 *Nat. Mater.* **6** 744
[12] Bucay J, Roussel E, Vasseur J O, Deymier P A, Hladky-Hennion A C, Pennec Y, Muralidharan K, Djafari-Rouhani B and Dubus B 2009 *Phys. Rev. B* **79** 214305
[13] Bringuier S, Swinteck N, Vasseur J O, Robillard J F, Runge K, Muralidharan K and Deymier P A 2011 *J. Acoust. Soc. Am.* **130** 1919
[14] Swinteck N, Robillard J F, Bringuier S, Bucay J, Muralidharan K, Vasseur J O, Runge K and Deymier P A 2011 *Appl. Phys. Lett.* **98** 103508
[15] Swinteck N, Bringuier S, Robillard J F, Vasseur J O, Hladky-Hennion A C, Runge K and Deymier P A 2011 *J. Appl. Phys.* **110** 074507
[16] Espinosa V, Sánchez-Morcillo V J, Staliunas K, Pérez-Arjona I and Redondo J 2007 *Phys. Rev. B* **76** 140302
[17] Pérez-Arjona I, Sánchez-Morcillo V J, Redondo J, Espinosa V and Staliunas K 2007 *Phys. Rev. B* **75** 014304
[18] Soliveres E, Espinosa V, Pérez-Arjona I, Sánchez-Morcillo V J and Staliunas K 2009 *Appl. Phys. Lett.* **94** 164101
[19] Chiang C Y and Luan P G 2010 *J. Phys.: Condens. Matter* **22** 055405
[20] Sánchez-Morcillo V J, Staliunas K, Espinosa V, Pérez-Arjona I, Redondo J and Soliveres E 2009 *Phys. Rev. B* **80** 134303
[21] Picó R, Sánchez-Morcillo V J, Pérez-Arjona I and Staliunas K 2012 *Appl. Acoust.* **73** 302
[22] Li X F, Ni X, Feng L, Lu M H, He C and Chen Y F 2011 *Phys. Rev. Lett.* **106** 084301
[23] Cicek A, Kaya O A and Ulug B 2012 *Appl. Phys. Lett.* **100** 111905
[24] Feng L, Liu X P, Chen Y B, Huang Z P, Mao Y W, Chen Y F, Zi J and Zhu Y Y 2005 *Phys. Rev. B* **72** 033108
[25] Feng L, Liu X P, Lu M H, Chen Y B, Chen Y F, Mao Y W, Zi J, Zhu Y Y, Zhu S N and Ming N B 2006 *Phys. Rev. Lett.* **96** 014301
[26] Berenger J P 1994 *J. Comput. Phys.* **114** 185